Gas Fluidization Characteristics of Nanoparticle Agglomerates

Chao Zhu, Qun Yu, and Rajesh N. Dave
Dept. of Mechanical Engineering, New Jersey Institute of Technology, Newark, NJ 07102

Robert Pfeffer
Dept. of Chemical Engineering, New Jersey Institute of Technology, Newark, NJ 07102

DOI 10.1002/aic.10319
Published online in Wiley InterScience (www.interscience.wiley.com).

An experimental study is conducted to determine the effect of different types of nanoparticles on the gas fluidization characteristics of nanoparticle agglomerates. Taking advantage of the extremely high porosity of the bed, optical techniques are used to visualize the flow behavior, as well as to measure the sizes of the fluidized nanoparticle agglomerates at the bed surface. Upon fluidizing 11 different nanoparticle materials, two types of nanoparticle fluidization behavior, agglomerate particulate fluidization (APF) and agglomerate bubbling fluidization (ABF), are observed and systematically investigated. A simple analytical model is developed to predict the agglomerate sizes for APF nanoparticles, and the results agree fairly well with the optical measurements. Using the Ergun equation, the experimentally measured pressure drop and bed height, and the average agglomerate size and voidage at minimum fluidization predicted by the model, the minimum fluidization velocities for APF nanoparticles are calculated and also agree well with the experimental values. Other important fluidization features such as bed expansion, bed pressure drop, and hysteresis effects, and the effects of the primary particle size and material properties are also described. © 2005 American Institute of Chemical Engineers
AIChE J, 51: 426–439, 2005
Keywords: fluidization, nanoparticles, agglomerates, pressure drop, bed expansion

Introduction

Gas fluidization of small solid particles has been widely used in a variety of industrial applications because of its unusual capability of continuous powder handling, good mixing, large gas–solid contact area, and very high rates of heat and mass transfer. Extensive research has been done in the area of gas fluidization, and the fluidization behavior of classical powders in the size range of 30 to 1000 μm (Geldart group A and B powders) is relatively well understood. However, the fluidization behavior of ultrafine particles, including nanoparticles, is much more complex and has received relatively little attention in the literature.

Because of their unique properties arising from their very small primary particle size and very large surface area per unit mass, nanostructured materials are already being used in the manufacture of drugs, cosmetics, foods, plastics, catalysts, energetic and biomaterials, and in mechatronics and micro-electro-mechanical systems (MEMS). Therefore, it is necessary to develop processing technologies that can handle large quantities of nanosized particles, such as mixing, transporting, modifying the surface properties (coating), and downstream processing of nanoparticles to form nanocomposites. Before processing of nanostructured materials can take place, however, the nanosized particles have to be well dispersed. Gas fluidization is one of the best techniques available to disperse

Correspondence concerning this article should be addressed to R. Pfeffer at pfeffer@adm.njit.edu.

and process powders belonging to the Geldart group A and B classifications. Based on their primary particle size and material density, however, nanosized powders fall under the Geldart group C (<30 microns) classification, which means that fluidization is expected to be difficult because of cohesive forces that become more prominent as the particle size decreases.

Because of the strong interparticle forces that exist between them (such as van der Waals, electrostatic, and moisture-induced surface tension forces), nanoparticles are always found to be in the form of large-sized agglomerates, rather than as individual nanosized particles when packed together in a gaseous medium. Thus, gas fluidization of nanoparticles actually refers to the fluidization of nanoparticle agglomerates.

Previous studies of gas fluidization of nanoparticle agglomerates[1-17] have found that minimum fluidization velocity is relatively high (about several orders of magnitude higher than the minimum fluidization velocity of primary nanoparticles[1,2,5-8,12,17]). The size of the fluidized nanoparticle agglomerates is typically from about 100 to 700 μm, whereas the primary particle size ranges from 7 to 500 nm.[1,2,8,11,12,16] For some nanoparticles, very smooth fluidization occurs with extremely high bed expansion, practically no bubbles are observed, and the velocity as a function of voidage around the fluidized agglomerates obeys the Richardson–Zaki equation.[1,2,5,6,8] This type of fluidization of nanoparticle agglomerates has been termed *agglomerate particulate fluidization* (APF) by Wang et al.[8] For other nanoparticles, fluidization results in a very limited bed expansion, and large bubbles rise up very quickly through the bed.[5,6] This type of fluidization has been termed *agglomerate bubbling fluidization* (ABF).[8] However, even for the homogeneously fluidized nanoparticles, relatively large powder elutriation occurs at the high gas velocities required to fluidize the nanoagglomerates. This loss of particles may hinder the applicability of fluidization of nanoparticle agglomerates in industrial processes.

In addition to conventional gravity-driven fluidization, nanoparticle agglomerates can also be fluidized in a rotating or centrifugal fluidized bed,[3,4,10] where the centrifugal force acting on the agglomerates can be set much higher than gravity. It is also found that the minimum fluidization velocity of nanoparticle agglomerates in a conventional fluidized bed can be significantly reduced by introducing external force excitations to the bed, such as vertical, sinusoidal vibration,[9] sound waves at relatively low frequency generated by a loudspeaker,[18] or applying an oscillating magnetic field to the nanoparticles that have been premixed with some very large (0.5–3 mm) magnetic particles.[19] With a much lower fluidizing gas velocity, hardly any elutriation of nanoparticles[9,18,19] was observed.

A number of studies dealing with modeling and numerical simulation of the fluidization of nanoparticle agglomerates can be found in the literature. These models are based either on force[1,11,16] or on energy[2,4] balances around individual agglomerates, the use of the Richardson–Zaki equation,[8] or a combination of the Richardson–Zaki equation with fractal analysis[9] for APF fluidization, or a modified kinetic theory.[12] Recently, some applications of nanoparticle agglomerate fluidization were investigated, including the production of carbon nanotubes,[14] and its application to photocatalytic NO_x treatment.[15]

However, very little experimental data on the fluidization characteristics and differences between APF and ABF nanoparticles, such as minimum fluidization velocity, agglomerate size, hysteresis effects, and the effect of nanoparticle material properties, are available, which calls for a systematic and experimental study of various nanoparticle materials. The primary objective of this study therefore is to experimentally determine the fluidization characteristics of a variety of different nanoparticles and to correlate the macroscopic fluidization behavior (APF or ABF) of the nanoagglomerates with the properties of the primary nanoparticles in a conventional gravity-driven fluidized bed without any additional external forces present. Another task is to develop a simple and effective method to estimate the average size of the agglomerates and the bed voidage around the agglomerates, which can then be used in models to determine the minimum fluidization velocity, pressure drop, and other pertinent variables of the fluidization process.

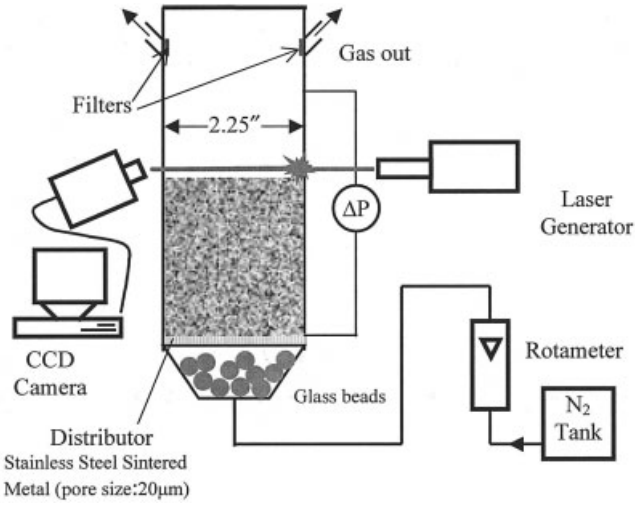

Figure 1. Experimental system.

Experimental Methods

A schematic diagram of the experimental fluidization system is shown in Figure 1. The system consists of a fluidized bed of nanoparticle agglomerates, flow and pressure measurement devices, a flow visualization system, and an optical sensor system for in situ size measurement of agglomerates. The fluidized bed is a vertical transparent column with a distributor at the bottom, consisting of a sintered stainless steel metal plate 2 mm thick having a pore size of 20 μm. The column is a section of acrylic pipe with an inner diameter of 57 mm and a height of 910 mm. To generate a uniform gas field, glass beads of diameter between 2.5 and 3.5 mm are charged into a chamber placed below the distributor and above the gas inlet to form a packed bed about 100 mm high. An ultrafine mesh filter is located at the gas outlet to filter out any elutriated nanoparticle agglomerates. The flow fluidization structure is visualized with the aid of a lighting device (Model 150SX; Illumination Technologies), recorded by a digital camcorder (Digital 8; Sony), and analyzed by a PC-based image-processing software. In situ images of fluidized agglomerates are obtained with the aid of a laser source (Laser Physics Reliant 1000m) focused on the fluidized bed surface, a CCD camera (LaVision FlowMaster 3S), and an image-processing system (Dual Xeon CPU).

Table 1. Properties of Nanoparticles*

Powder	Wettability	BET (m^2/g)	Size (nm)	Bulk Density (kg/m^3)	Material	Material Density (kg/m^3)	Fluidization Type	Surface Modification	Measured U_{mf} (cm/s)
R974	Hydrophobic	170	12	33.24	SiO_2	2560	APF	DDS	0.23
R805	Hydrophobic	150	12	45.88	SiO_2	2560	APF	DDS	0.65
R104	Hydrophobic	150	12	62.90	SiO_2	2560	APF	OCS	0.43
R711	Hydrophobic	150	12	45.88	SiO_2	2560	APF	MCS	0.38
COK84	Hydrophobic	170	12	37.86	SiO_2–Al_2O_3:7–1	2740	APF	None	1.26
R106	Hydrophobic	250	7	41.49	SiO_2	2560	APF	OCS	0.23
A 300	Hydrophilic	300	7	39.00	SiO_2	2560	APF	None	1.10
R972	Hydrophobic	110	16	39.00	SiO_2	2560	APF	DDS	0.29
OX50	Hydrophilic	50	40	121.33	SiO_2	2560	ABF	None	4.03
A 90	Hydrophilic	90	20	52.00	SiO_2	2560	ABF	None	7.71
TiO_2	Hydrophilic	50	21	128.29	TiO_2	4500	ABF	None	5.17

DDS; dimethyl-dichlorosilane; OCS, octamethylcy-clotetrasiloxane; MCS, methacrylsilane.

As shown in Table 1, 11 different nanoparticles of various materials, primary particle size, and surface modification are investigated in this study. Before the experiments, the particles were sieved using a shaker (Octagon 2000) and a 35-mesh sieve opening (about 500 μm). The sieving process serves to remove very large agglomerates that may have been generated during packing, storage, and transportation. However, it should be noted that even after sieving, because of fragmentation and reagglomeration during fluidization, some agglomerates in the bed might exceed the sieve openings.

The bulk densities of the different sieved nanoparticles varied from 30 to 130 kg/m^3. Because of surface treatment by the manufacturer, the nanoparticles are either hydrophobic or hydrophilic. To minimize any effect of humidity on the nanoparticle fluidization, pure dry nitrogen from a compressed nitrogen tank is used as the fluidizing gas. The gas flow rate is measured and adjusted by two calibrated rotameters (Gilmont) placed in parallel with a combined flow range of up to 30 L/min. The bed pressure drop is measured between the two pressure taps, one located at the top of the column near the flow exit and the other located slightly above (3 mm) the distributor, so that it is not necessary to measure the pressure drop across the distributor. A digital manometer (Cole Parmer) is used to measure lower pressure drops (up to 25 mm H_2O) and an inclined tube manometer (Dewyer Mark-II) is used for higher pressure drops.

Results and Discussion

Fluidization behavior

As discussed earlier, nanoparticles cannot be fluidized discretely, but fluidize in the form of large porous agglomerates as a result of the very strong interaction forces between them. Typical fluidization curves, that is, bed expansion and pressure drop curves, for APF and ABF nanoparticles are shown in Figures 2 and 3, respectively. For both APF and ABF nanoparticle agglomerates, the pressure drop increases with increasing superficial gas velocity and then reaches a plateau and becomes independent of the gas velocity. The value of the pressure drop plateau is usually close to the weight of the bed per unit area, indicating that the total weight of the particles is balanced by the pressure drop, all of the solid particles are suspended, and the bed is fully fluidized. The critical velocity beyond which a pressure drop plateau is reached is commonly called the *minimum fluidization velocity*.

For APF nanoparticles, we observed that the bed fluidizes and expands very uniformly without bubbles with a large expansion ratio of up to 500% or more, the bed expansion increases with increasing gas velocity, and the agglomerates distribute uniformly within the bed. Figure 2 shows that the bed starts to expand at a gas velocity much smaller than the minimum fluidization velocity as defined above; thus the bed appears to exhibit a fluidlike behavior at velocities much lower than the minimum fluidization velocity. As shown in Figure 3, for ABF nanoparticles, the bed expands very little with increasing gas velocity ($<$50%), and we observe large bubbles rising up very quickly through the bed; the agglomerates distribute nonuniformly within the bed and the smaller agglomerates appear to be smoothly fluidized in the upper part of the bed, whereas the larger agglomerates could be found moving slowly at the bottom.

Based on our experiments, we believe that the difference in fluidization behavior between APF and ABF depends largely on the bulk density and the primary particle size. The fluidization of relatively small ($<$20 nm) nanoparticles with a bulk density $<$ 100 kg/m^3 (see Table 1) appear to behave as APF, whereas larger and heavier nanoparticles are likely to behave as ABF. Similar results were observed in the experiments of Wang et al.[8]

Hysteresis phenomena and definition of minimum fluidization velocity

If the measured pressure drop or bed height depends on whether the velocity is increased (from a packed bed to a fluidized bed) or decreased (from a fluidized bed to a packed bed), a hysteresis phenomenon is observed.[20-22] A theoretical explanation for the hysteresis of the observed pressure drop during the fluidization and defluidization cycles based on the role of contact or yield stresses and wall friction, which results in plugging or channeling of the nanoparticle agglomerates at low velocities, is presented in Loezos et al.[23] and Tsinontides and Jackson.[24] We observed some hysteresis in the pressure drop and bed height measurements for all of the 11 different nanoparticle agglomerates used in this study, but different nanoparticle agglomerates show substantial differences in the hysteresis curves obtained (see Figures 2 and 3). For example, for some nanoparticles, such as Degussa Aerosil® R974, the pressure drop curves for both the fluidization branch and the defluidization branch are quite close, and the hysteresis phe-

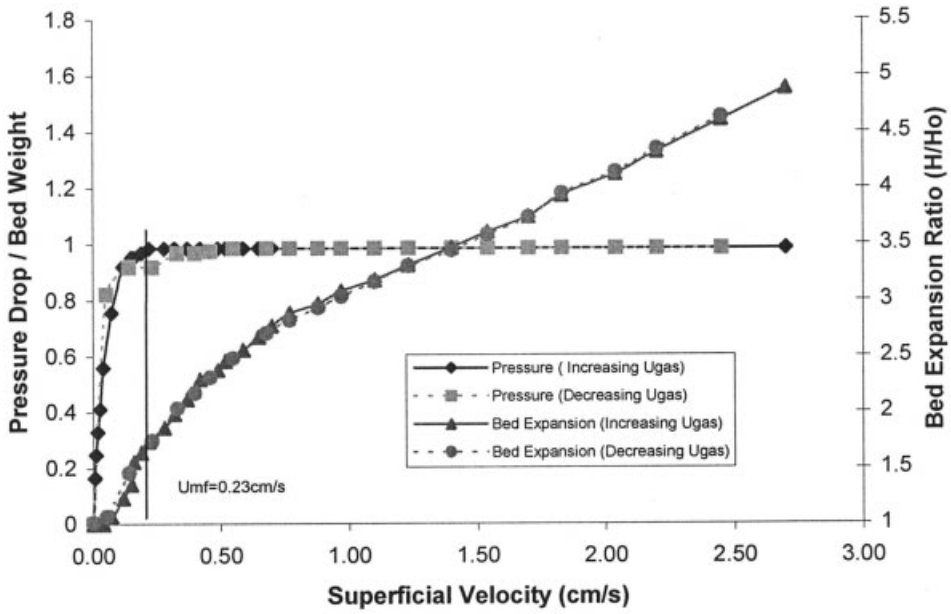

a. Degussa Aerosil® R974

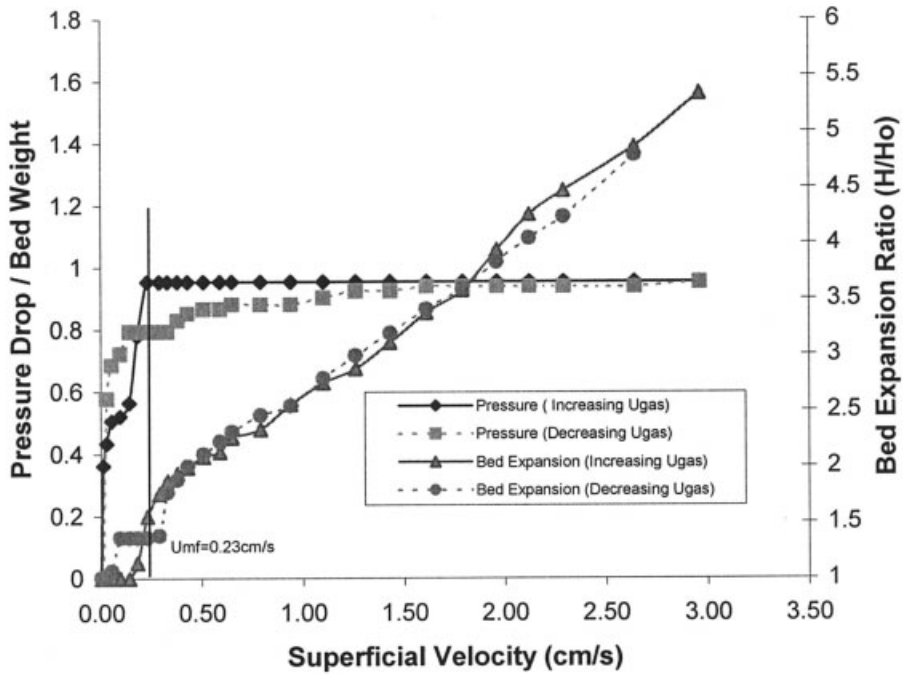

Figure 2. Typical fluidization curves for APF nanoparticles.

(a) Degussa Aerosil® R974; (b) Degussa Aerosil® R106.

nomenon is negligible; however, for other nanoparticles, such as Degussa Aerosil® titanium dioxide P25, the deviation of the pressure drop curves for the fluidization and defluidization branch is fairly large.

When the superficial gas velocity is decreased after the bed has been fluidized, the pressure drop will first remain constant, and then decline upon a further decrease in gas velocity, indicating defluidization has occurred. We observe, however, that for some nanoparticles the pressure drop begins to decline upon decreasing the gas velocity, even though the bed still appears to be fully fluidized (see Figure 2b) or remains at the plateau level at velocities much lower than those needed to

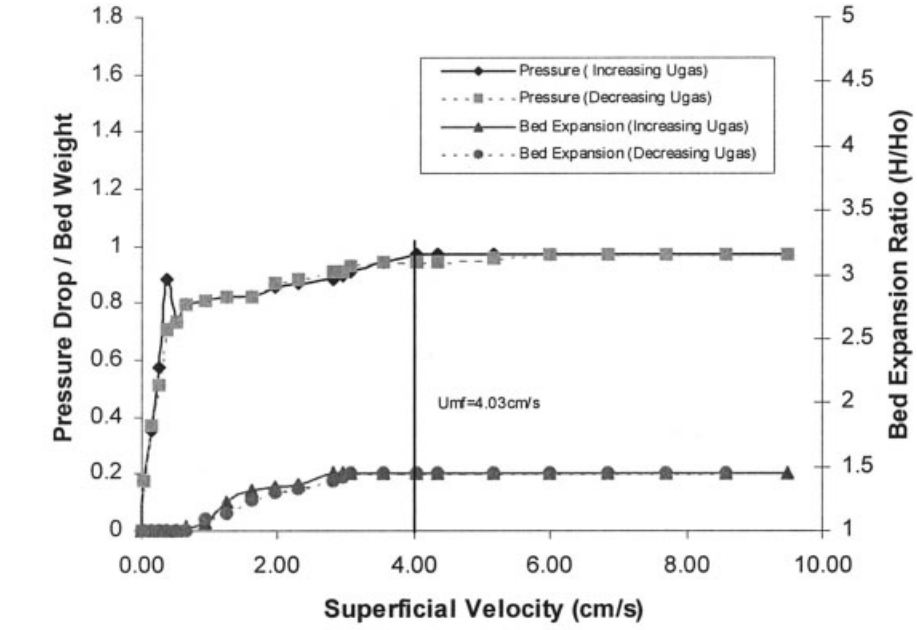

a. Degussa Aerosil ® OX50

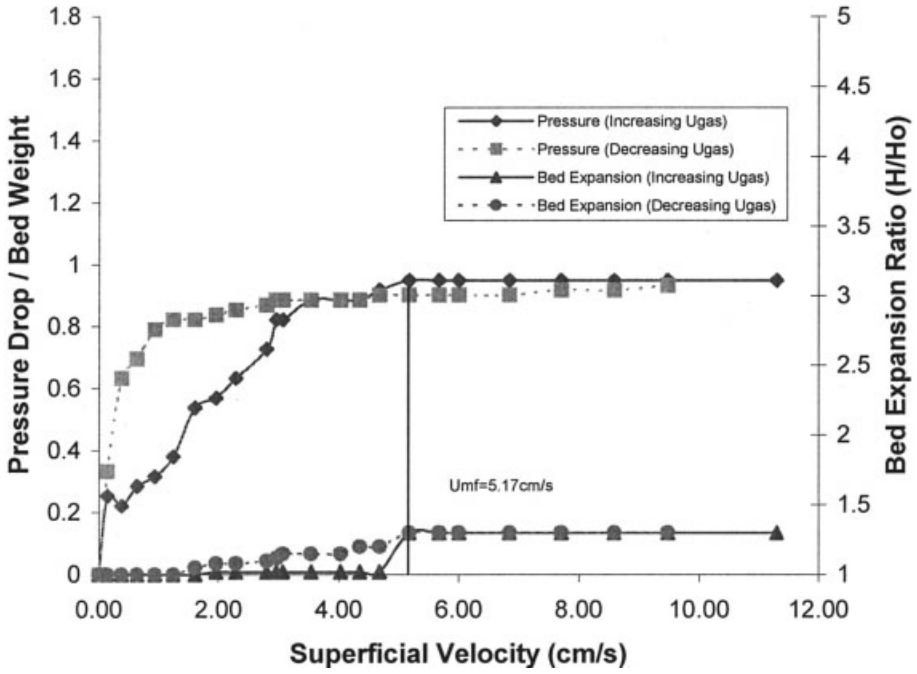

Figure 3. Typical fluidization curves for ABF nanoparticles.

(a) Degussa Aerosil® OX50; (b) Degussa titanium dioxide P25.

attain fluidization (see Figure 3b). Thus, in this study, we have chosen the fluidization branch of the pressure drop cycle as the reference to define the minimum fluidization velocity as the superficial gas velocity beyond which the bed pressure drop is no longer dependent on velocity and becomes constant.

Agglomerate size for APF nanoparticles

Agglomerate size is one of the key factors that influence the fluidization behaviors of nanoparticles, and models to predict the agglomerate size have been proposed for cohesive micron-size particles[11,16,25] and for nanoparticles.[2,8,9] We have also

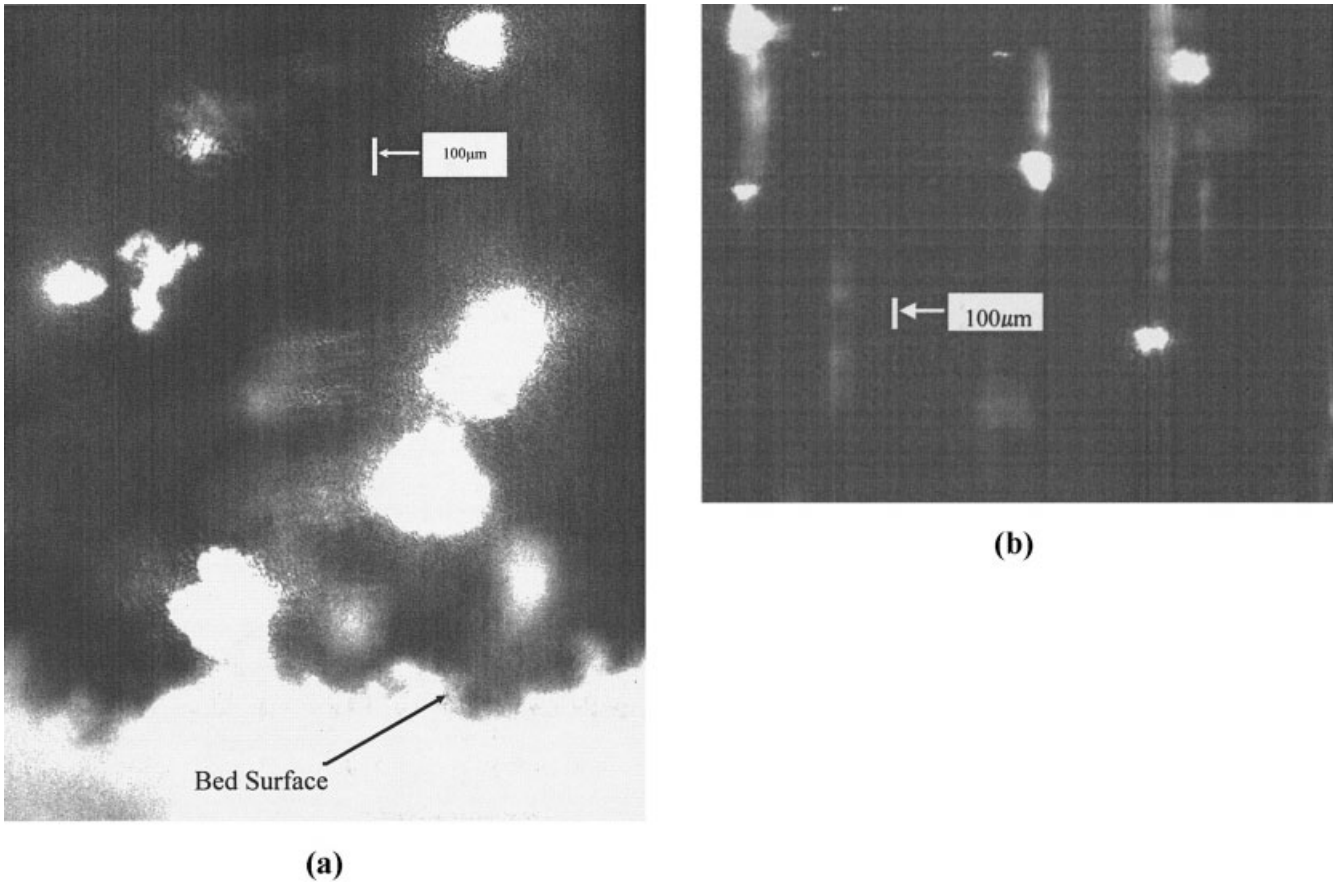

Figure 4. (a) Images of APF nanoagglomerates near the fluidized bed surface (Degussa Aerosil® R974); (b) images of ABF nanoagglomerates near the fluidized bed surface (Degussa titanium dioxide P25).

obtained in situ measurements of agglomerate size in a fluidized bed of nanoparticles, using an optical system to image the agglomerates on the surface of the fluidized bed.[9,18]

We used this optical system to obtain an approximate size analysis of 10 of our 11 different nanoagglomerates. We were unable to measure the agglomerate size of the OX50 nanoparticles because they tend to stick to the wall of the vessel and were optically too dense to produce acceptable images. Thus we estimated their mean size as 300 μm based on the experimental results of the other 10 nanoparticles. Figure 4 shows typical images of the APF and ABF agglomerates on the fluidized bed surface. The images show that the agglomerates are not spherical but, because of the random orientation of the irregular agglomerates in the gas flow, we assume that the agglomerates can be represented as spheres. Figure 5 shows the size distribution of one type of nanoparticles studied; Table 2 summarizes the results for all of the other nanoparticles.

Chaouki et al.[1] proposed a model based on a hydrodynamic force balance to predict the agglomerate size in a fluidized bed, and later on, Morooka et al.[2] proposed a model based on an energy analysis to predict the agglomerate size. Based on Chaouki's model and using the Richardson–Zaki equation, Wang et al.[8] were able to predict the agglomerate size of a variety of silica nanoparticles in a fluidized bed. Nam et al.[9] developed an innovative fractal analysis method to predict the size of nanoparticle agglomerates. In this study, a new model to predict agglomerate size for APF nanoparticles will be proposed based on the Richardson–Zaki equation.

It is well known that the Richardson–Zaki equation and the Ergun equation are applicable for solid (nonpermeable) particles, but whether these equations are still valid for permeable nanoparticle agglomerates has not been addressed in the previous literature. We have shown (see the Appendix) that the error in assuming that the nanoparticle agglomerates behave as solid particles for the purposes of hydrodynamic analysis is very small for ABF nanoparticles, and is also small for APF nanoparticles when they fluidize at very high bed expansions.

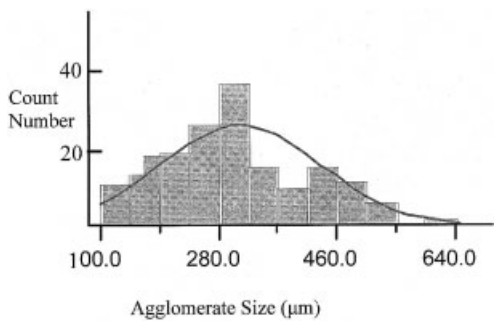

Figure 5. Typical agglomerate size distribution.

Degussa Aerosil® R974.

Table 2. Statistics of Measured Agglomerate Sizes

Powder	Sampling Number	Experimental Agglomerate Mean Size (μm)	Standard Error Mean (μm)	Upper 95% Mean (μm)	Lower 95% Mean (μm)
R974	193	315	8.8	333	298
R805	108	218	7.9	234	202
R104	427	226	3.7	233	219
R711	250	274	10.8	296	253
COK84	59	320	20.9	362	278
R106	179	172	5.7	183	160
A 300	230	585	15.7	616	554
R972	139	422	15.2	452	392
A 90	189	896	33.2	961	830
TiO_2	144	195	5.4	205	184
OX50	Unable to measure agglomerate size.				

This implies that the Richardson–Zaki and Ergun equations derived for solid particles should be applicable to these porous nanoparticle agglomerates.

By ignoring any elutriation and/or adhesion on the walls of the vessel, an overall mass balance on the powder in the fluidized bed is given by

$$\rho_a(1 - \varepsilon_g) HA = \rho_b H_0 A = \rho_{a0}(1 - \varepsilon_{g0}) H_0 A \qquad (1)$$

where ρ_a is the bulk density of the agglomerates and ε_g is the bed voidage around the agglomerates. It should be noted that ε_g excludes the voidage within the agglomerates themselves. In the model of Wang et al.,[8] they assume that $\rho_a \approx \rho_b$ so that

$$(1 - \varepsilon_g) = H_0/H \qquad (8a)$$

and the initial bed voidage (when $H = H_0$) $\varepsilon_{g0} = 0$ or $\alpha_{p0} = 1$, which is physically unrealistic. When the nanoparticle agglomerates are loosely packed in the fluidizing vessel (chamber), the volume fraction of the agglomerates can never reach 1 ($\varepsilon_{g0} = 0$), and the specific value will depend on the particle size distribution, sphericity of the particles, packing method, dimensions of the chamber, surface interaction with the chamber, and other factors.

Normally, for "hard" solid particles, the typical bed voidage ε_{g0} in a loose packed bed is within the range of 0.35 to 0.5.[26] However, for highly deformable particles (such as clay) and/or particles of different sizes, the voidage can be very much smaller.[26] Therefore, because of the highly porous and fragile structure of the nanoparticle agglomerates, and the relatively wide particle size distribution, it is possible that the initial packed bed voidage is much lower than the typical voidage of monodisperse hard solid particles.

Although the fragile nanoagglomerates show dynamic behavior, in that they are continuously breaking into smaller agglomerates and reagglomerating into larger ones, there is no evidence that the density of the agglomerates undergoes any appreciable change during fluidization. Therefore, an important assumption, which we make, is that for a nanoparticle bed, the density of the agglomerates ρ_a remains almost constant before and during the fluidization so that

$$\rho_a \approx \rho_{a0} \qquad (2)$$

and Eq. 1 can be written in the form

$$\varepsilon_g = 1 - \frac{H_0}{H}(1 - \varepsilon_{g0}) \qquad (3)$$

We have already shown that the porous agglomerates could be treated as solid particles (see the Appendix) and the Reynolds number for APF nanoparticle agglomerates is <1 (see Table 6 below) so that Stokes flow (creeping motion) prevails. Because we have observed that APF nanoparticle agglomerates fluidize smoothly without any bubbles, and behave similar to particles fluidized by liquids, we also assume that the well-known Richardson–Zaki equation is valid. This equation relates the superficial gas velocity U_g with the bed voidage (around the agglomerates) and the terminal velocity for a single agglomerate U_{pt} as

$$U_g = U_{pt}\varepsilon_g^n \qquad (4)$$

Davis and Birdsell[27] showed that a Richardson–Zaki exponent of $n = 5.0 \pm 0.1$ should be used for the Stokes-flow regime. Nam et al.[9] have also shown that a Richardson–Zaki exponent of $n = 5$ is valid for APF nanoparticle agglomerates.

By combining Eqs. 3 and 4, the relation between the superficial gas velocity and the particle terminal velocity can be written as

$$U_{pt}^{1/n} - U_{pt}^{1/n}(1 - \varepsilon_{g0})\frac{H_0}{H} = U_g^{1/n} \qquad (5)$$

which reduces to a linear equation

$$y = B - Ax \qquad (6)$$

where

$$y = U_g^{1/n} \qquad x = \frac{H_0}{H} \qquad A = U_{pt}^{1/n}(1 - \varepsilon_{g0}) \qquad B = U_{pt}^{1/n} \qquad (7)$$

Thus, for each of the APF nanoparticle agglomerates, a plot of $U_g^{1/n}$ vs. H_0/H can be drawn, and from a linear regression, the slope $-A$ and the y-intercept B can be found. From these values the particle terminal velocity U_{pt} and the initial bed voidage ε_{g0} can be calculated as

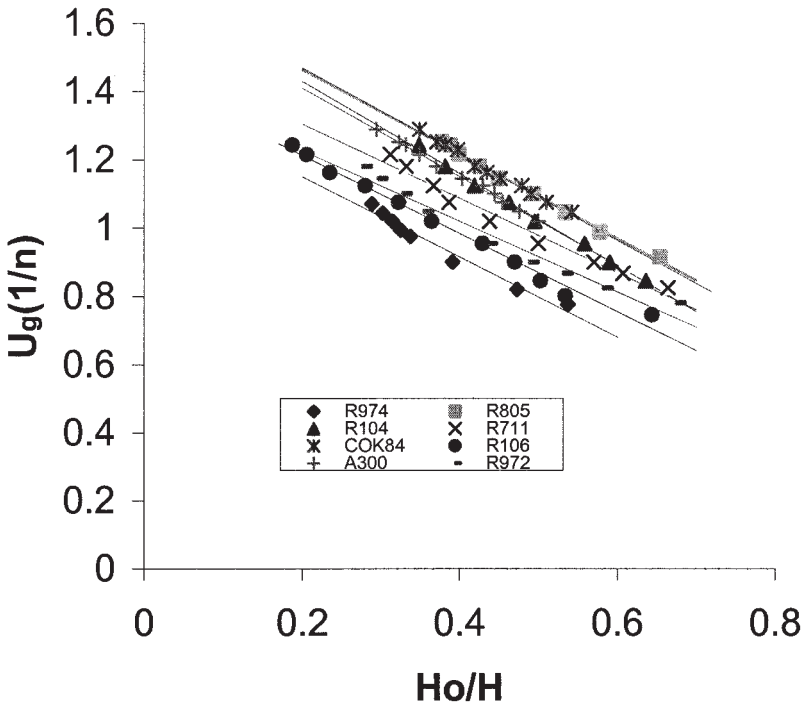

Figure 6. $U_g^{1/n}$ vs. H_0/H for eight different APF nanoparticles.

Solid lines are linear regression results, and data points are experimental results, for a Richardson–Zaki exponent $n = 5$.

$$U_{pt} = B^n \tag{8}$$

$$\varepsilon_{g0} = 1 - \frac{A}{B} \tag{9}$$

Figure 6 is a plot of $U_{pt}^{1/n}$ vs. H_0/H for the eight different APF nanoparticles, with $n = 5$; all of the data points fall within the zone between the inner and outer solid lines. The figure also shows that all of the straight lines (for each of the eight nanoparticle agglomerates) intersect the y-axis fairly close to each other, indicating that the terminal velocities for these eight nanoparticles are roughly of the same order of magnitude. The curves for each of the nanoparticles also have similar slopes, and because the terminal velocities are close to each other, the initial bed voidages are also close to one another. The linear regression results for the initial voidage ε_{g0} are listed in Table 3; for the eight nanoparticles, the mean initial bed voidage ε_{g0} is 0.237, with a standard deviation of only 0.046.

Table 3. Calculated Agglomerate Sizes and Initial Bed Voidage for APF Nanoparticles ($n = 5$)

Powder	U_{pt} (cm/s) Calculated	ε_{g0} Calculated	d_a (μm) Calculated	d_a (μm) Measured
R974	5.09	0.152	211	315
R805	14.6	0.277	279	218
R104	14.1	0.206	245	226
R711	8.16	0.285	207	274
COK84	15.1	0.266	316	320
R106	6.21	0.206	201	172
A 300	12.9	0.223	296	585
R972	6.04	0.278	195	422
Mean		0.237 (SD = 0.046)		

From the experimental measurement results shown in Table 2, the agglomerates have a wide size distribution: the largest agglomerates of R974 are as much as 10 times larger than the smallest. According to Fayed and Otten,[26] packing a mixture of spherical particles of different sizes could result in very low bed voidages, as low as 0.207 for two different sized spheres with a size ratio of 0.414, and even lower for many different sized particles including fines. Therefore, it may be possible that the fragile, highly porous, APF nanoparticles, will pack at an initial bed voidage ε_{g0} between 0.2 and 0.25, as predicted by our model (Figure 6).

Figure 7 is a plot of the superficial gas velocity U_g vs. the bed expansion ratio H/H_0 for the eight different group A–like nanoparticles with a Richardson–Zaki exponent $n = 5$ and Figure 8 is a classical logarithmic plot of the bed voidage vs. the superficial velocity.

From the values of U_{pt}, obtained from the y-intercepts in Figure 6 and assuming Stokes law, the average size of the agglomerates can be calculated from

$$d_a = \sqrt{\frac{18\mu U_{pt}}{(\rho_a - \rho)g}} \tag{10}$$

where $\rho_g = 1.205$ kg/m^3, and $\mu = 1.81 \times 10^{-5}$ Pa·s (atmospheric pressure and 20°C). These values are listed in Table 3 and most of the results compare reasonably well with the experimentally measured values, although some differ by as much as a factor of 2. Given the limitations of the measurement technique and uncertainties in the model assumptions, this discrepancy is quite satisfactory. However, both the calculated and experimental mean sizes of the fluidized nanoparticle ag-

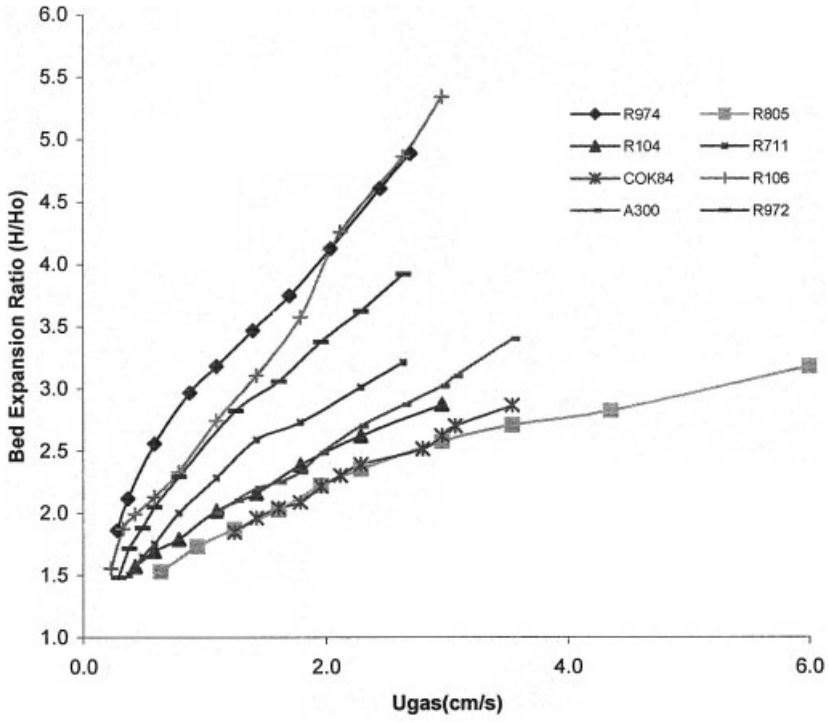

Figure 7. Bed expansion ratio as a function of superficial gas velocity for APF nanoparticles.

glomerates are within 200 to 600 μm, which are at least four orders of magnitude larger than the primary particle sizes.

To investigate the sensitivity of the Richardson–Zaki exponent on the calculated mean agglomerate size, we chose two different values of n, 4 and 6, and repeated the linear regression analysis. Table 4 shows the calculated results for the mean agglomerate diameters for n values of 4, 5, and 6. Surprisingly, the diameter of the agglomerates was found to be relatively insensitive to the value of the Richardson–Zaki exponent. For example, for R974 nanoparticles, the mean agglomerate size is 217 μm for $n = 4$, 211 μm for $n = 5$, and 204 μm for $n = 6$, respectively. Nam et al.[9] also studied the sensitivity of the

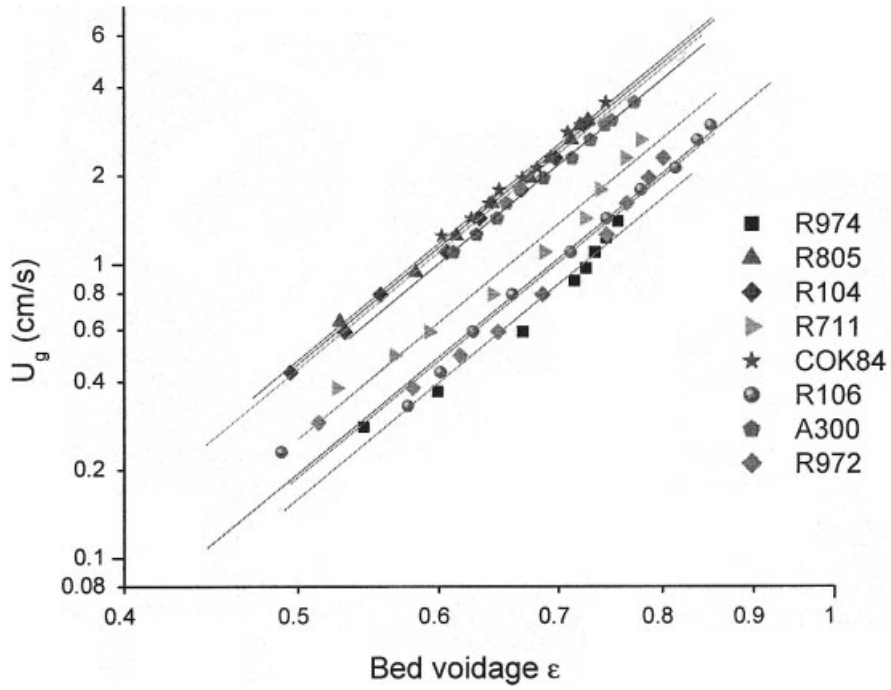

Figure 8. Bed voidage vs. superficial gas velocity for APF nanoparticles.

Solid lines are linear regression results, and data points are experimental results for a Richardson–Zaki exponent $n = 5$.

Table 4. Mean Agglomerate Size for APF Nanoparticles

	d_a (μm)		
Powder	$n = 4$	$n = 5$	$n = 6$
R974	218	211	204
R805	285	279	273
R104	247	245	242
R711	214	207	201
COK84	327	316	304
R106	210	201	193
A 300	309	296	284
R972	202	195	188

value of n, and drew a similar conclusion. Table 5 shows a comparison of the results for the mean agglomerate size based on our model with those obtained from the fractal analysis model proposed by Nam et al.[9] for all three values of n, 4, 5, and 6; the difference is within 2%, which lends confidence to using our simpler model for predicting the agglomerate size of APF nanoparticles. It should be noted, however, that the model cannot be used to predict the mean agglomerate size of ABF nanoparticles.

Minimum fluidization velocity for APF and ABF nanoparticles

For APF nanoparticles at low Reynolds numbers, the minimum fluidization velocity U_{mf} can be calculated from the following simplified Ergun equation

$$U_{mf} = \frac{\Delta P}{H} \frac{d_a^2}{150\mu} \frac{\varepsilon_{gmf}^3}{(1 - \varepsilon_{gmf})^2} \tag{11}$$

Here we use the measured pressure drop and bed height at minimum fluidization (obtained from plots similar to Figure 2 for each of the APF nanoparticles), d_a calculated from Eq. 10, and values of ε_{gmf} taken from Figure 8 at the minimum fluidization velocity U_{mf}. The calculated minimum fluidization velocities are compared with the experimental measurements in Table 6, which shows a fairly good agreement between the two. Table 6 also lists the Reynolds numbers for each of the APF nanoparticles (ranging from 0.05 to 0.35 and thus in the creeping motion regime), and the bed expansion ratios at the minimum fluidization velocity.

Table 7 gives the measured mean agglomerate size, minimum fluidization velocity, and the bed expansion ratio and Reynolds number at minimum fluidization for the three ABF nanoparticles. In addition to exhibiting much lower bed expansions and much higher minimum fluidization velocities, these nanoagglomerates also have much higher Reynolds numbers (1.7 to 16) at minimum fluidization.

We also note from from Table 1, the average U_{mf} of the six hydrophobic (attributed to surface modification) APF nanoparticles (Degussa Aerosil® R974, R805, R104, R711, R106, R972) is 0.37 cm/s, whereas the average U_{mf} for the two hydrophilic (without surface modification) nanoparticles (Degussa Aerosil® COK84, A300) is much higher at 1.18 cm/s. This difference is probably a result of the better flowability of the hydrophobic nanoparticles after surface modification. There may also be some moisture trapped within the hydrophilic particles, making them more cohesive than the hydrophobic particles.

Classification criterion to differentiate between APF and ABF nanoparticles

Earlier in this article we stated that the difference in fluidization behavior between smooth, liquidlike, bubbleless, particulate fluidization with high bed expansion (APF), and nonhomogeneous, bubbling, aggregative fluidization with low bed expansion (ABF) depends largely on the bulk density and the primary particle size. Based on our experimental results, we concluded that the fluidization of relatively small (<20 nm) nanoparticles with a bulk density < 100 kg/m^3 (see Table 1) appear to behave as APF, whereas larger and heavier nanoparticles are likely to behave as ABF.

On the basis of experimental data using classical fluidized particles such as FCC catalyst, UOP catalyst, and hollow resin, Romero and Johanson[28] present a criterion to characterize the quality of fluidization as either smooth or bubbling, depending on the value of a combination of dimensionless groups. These dimensionless groups consist of the product (Π) of the particle to fluid density ratio, the Reynolds (Re) and Froude (Fr) numbers at minimum fluidization, and the bed height to bed diameter ratio

$$\Pi = \mathrm{Fr}_{mf}\mathrm{Re}_{mf} \frac{\rho_a - \rho_g}{\rho_g} \frac{H_{mf}}{d_t} < 100 \qquad \text{smooth fluidization}$$

$$\Pi = \mathrm{Fr}_{mf}\mathrm{Re}_{mf} \frac{\rho_a - \rho_g}{\rho_g} \frac{H_{mf}}{d_t} > 100 \qquad \text{bubbling fluidization}$$

Although our porous nanoparticle agglomerates behave in a manner different from that of the classical solid particles used to obtain Eq. 12, there are some definite similarities, and we calculated the values of the combination of dimensionless groups (which we designate as Π) for all 11 nanoparticles used in the experiments. To our surprise, the calculated results (see Tables 6 and 7) agree remarkably well with this criterion. For the eight APF nanoparticles, the values of Π are within the range of 0.008–1.55, which is much less than 100, whereas for the three ABF nanoparticles, the values of Π are within the range of 398–1441, which is much larger than 100. Thus, this criterion may also be valid for nanoparticle agglomerates, and therefore could be used to check whether a nanoparticle of interest will behave as APF or ABF. Of course, this hypothesis is based only on experimental data using 11 different nanoparticles, and more research is needed to confirm that this classification criterion is indeed applicable for all nanoparticles.

Table 5. Comparison of Models Used to Predict the Agglomerate Size of R974 Nanoparticles

	Agglomerate Diameter (μm)		
R974	Based on Present Model	Based on Fractal Analysis Model	Experimental Measurement
$n = 4$	218	214	315
$n = 5$	211	208	315
$n = 6$	204	202	315

Table 6. Fluidization Characteristics of APF Nanoparticles

Powder	Measured U_{mf} (cm/s)	Calculated U_{mf} (Eq. 11) (cm/s)	Measured H_{mf}/H_0	Re_{mf} $(\rho_a d_a V/\mu)$	Fr_{mf} $(u_{mf}^2/d_a g)$	$(\rho_a - \rho_g)/\rho_g$	H_{mf}/d_t	Π
R974	0.23	0.17	1.73	0.05	0.0013	31.7	3.71	0.008
R805	0.65	0.56	1.53	0.19	0.0109	51.9	2.27	0.246
R104	0.43	0.42	1.57	0.13	0.0068	65.0	3.41	0.197
R711	0.38	0.31	1.51	0.08	0.0045	52.5	2.24	0.043
COK84	1.26	0.94	1.84	0.35	0.0316	42.0	3.32	1.55
R106	0.23	0.17	1.55	0.05	0.0015	42.6	2.55	0.008
A 300	1.1	0.83	2.00	0.29	0.0288	40.8	3.5	1.19
R972	0.29	0.24	1.48	0.05	0.0021	44.1	2.2	0.010

Concluding Remarks

Highly porous nanoparticle agglomerates exhibit two distinct fluidization behaviors: APF (smooth fluidization without bubbles at minimum fluidization) and ABF (bubbles at minimum fluidization). APF agglomerates show very large bed expansions, up to five times the initial bed height as the superficial gas velocity is increased, and the Reynolds numbers for these nanoagglomerates at minimum fluidization are very low (0.05 to 0.35), which indicate that the agglomerates are in creeping flow. ABF nanoagglomerates fluidize with large bubbles and show very little bed expansion as the superficial gas velocity is increased and the Reynolds numbers at minimum fluidization are close to or higher than 2.0, indicating that hydrodynamic inertial effects cannot be neglected.

A model for a permeable sphere in a swarm of permeable spheres (see the Appendix), shows that fluidized APF nanoparticle agglomerates (at large ε_g) can be treated as solid particles for hydrodynamic analysis with little error, so that the Ergun and Richardson–Zaki equations derived for solid particles should also be applicable to these porous nanoparticle agglomerates. For APF nanoparticles, a model based on the initial bed voidage around the agglomerates and the Richardson–Zaki equation was used to predict the mean agglomerate size in the fluidized bed. The analysis is relatively insensitive to the value of the Richardson–Zaki exponent and we set $n = 5$ because the flow is in the creeping motion regime. We found that the initial bed voidage for the nanoparticle agglomerates is around 0.2 to 0.25, which is lower than the theoretical packing voidage of spheres of uniform size, but is reasonable for soft agglomerates of wide size distribution. An in situ optical measurement method is used to measure the agglomerate sizes on the fluidized bed surface and these compared fairly well with the results predicted by the model. Typical sizes of the nanoparticle agglomerates are within the range of 200 to 600 μm.

The Ergun equation, based on the agglomerate size and voidage at minimum fluidization predicted by the model, can be used to calculate the minimum fluidization velocity for APF nanoparticle agglomerates. The calculated results agree very well with the experimental results. It was also found that the hydrophobic nanoparticles with surface modification result in a lower minimum fluidization velocity compared to that of hydrophilic particles because of improved flowability.

A classification criterion based on the value of a combination of dimensionless groups to differentiate between particulate and bubbling fluidization for classical solid fluidized particles also appears to predict remarkably well whether nanoparticles will behave as APF or ABF. This criterion may be superior to simply using the size and bulk density of the nanoparticles to predict their fluidization behavior.

Acknowledgments

The authors acknowledge the National Science Foundation for financial support through Grant 0210400 (NIRT—Collaborative Research: Experimental and Computational Investigations of Fluid Interactions/Transport in Nanodomains and Around Nanoparticles). We also express our appreciation to Dr. Herbert Riemenschneider and Jonah Klein of Degussa-Huls for supplying us with nanoparticles, and to Dr. Guangliang Liu and Yueyang Sheng for assistance in taking images of nanoagglomerates on the fluidized bed surface.

Notation

C_D = drag coefficient for solid sphere in gas flow, dimensionless
d_a = average size of fluidized agglomerates, μm
d_{sub} = average size of subagglomerates, μm
d_t = diameter of vessel (chamber), cm
F_{Dp} = drag force exerted on a permeable sphere in a swarm of permeable spheres, N
F_{Ds} = drag force exerted on a solid sphere in a swarm of solid spheres, N
Fr_{mf} = Froude number at minimum fluidization velocity $(=u_{mf}^2/d_a g)$, dimensionless
g = gravitational constant, N m^{-1} s^{-2}
H = height of fluidized bed, cm
H = initial height of bed, cm
H_{mf} = bed height at minimum fluidization velocity, cm
k = permeability of porous sphere, m^2
n = exponent in the Richardson–Zaki equation, dimensionless
Re_{mf} = Reynolds number at minimum fluidization velocity, dimensionless
U_g = superficial gas velocity, m/s
U_{pt} = terminal velocity for a single agglomerate, m/s
U_{mf} = minimum fluidization velocity of agglomerates, m/s
V = superficial fluid velocity for the swarm, m/s

Table 7. Fluidization Characteristics of ABF Nanoparticles

Powder	Measured Agglomerate Size (μm)	Measured U_{mf} (cm/s)	Measured H_{mf}/H_0	Re_{mf} $(\rho_a d_a V/\mu)$	Fr_{mf} $(u_{mf}^2/d_a g)$	$(\rho_a - \rho_g)/\rho_g$	H_{mf}/d_t	Π
OX50	300*	4.03	1.44	1.81	0.552	131.	3.02	398
A 90	896	7.71	1.11	16.5	0.677	55.8	2.31	1441
TiO_2	195	5.17	1.3	1.74	1.4	139.	2.73	927

*Estimated, could not be measured.

Greek letters

β = permeability related dimensionless radius of sphere, dimensionless
η = a bed voidage–dependent parameter $(=1 - \varepsilon_g)^{1/3}$, dimensionless
ε_g = bed voidage around the agglomerates, dimensionless
ε_g = initial bed voidage around the agglomerates, dimensionless
ε_{gmf} = the value of ε_g at the minimum fluidization velocity, dimensionless
ε_g,*sub* = volume fraction of gas around subagglomerates in a single agglomerate, dimensionless
μ = viscosity of fluid, Pa·s
ρ_a = density of agglomerate in fluidized bed, kg/m^3
ρ_a = initial density of agglomerate in fluidized bed, kg/m^3
ρ_b = bulk density of bed, kg/m^3
ρ_g = density of gas, kg/m^3
ρ_m = material density of primary particle, kg/m^3
Ω_p = drag force correction factor for permeable spheres in a swarm of permeable spheres, dimensionless
Ω_s = drag force correction factor for solid spheres in a swarm of solid spheres, dimensionless
Ω = ratio of F_{Dp} to F_{Ds} $(\equiv F_{Dp}/F_{Ds} = \Omega_p/\Omega_s)$, dimensionless
Π = $\mathrm{Fr}_{mf}\mathrm{Re}_{mf}$ $\{[(\rho_a - \rho_g)/\rho_g](H_{mf}/d_t)\}$, dimensionless

Literature Cited

1. Chaouki J, Chavarie C, Klvana D. Effect of interparticle forces on the hydrodynamic behavior of fluidized aerogels. *Powder Technol*. 1985; 43:117-125.
2. Morooka S, Kusakabe K, Kobata A, Kato Y. Fluidization state of ultrafine powders. *J. Chem. Eng. Jpn.* 1988;21:41-46.
3. Matsuda S, Hatano H, Muramota T, Tsutsumi A. Particle and bubble behavior in ultrafine particle fluidization with high G. In: Kwauk M, Li J, Yang W-C, eds. *Fluidization X*, Proc. 10th Eng. Found. Conf. Fluidization, Beijing, China; 2001:501-508.
4. Matsuda S, Hatano H, Tsutsumi A. Modeling for size reduction of agglomerates in nanoparticle fluidization, Proc. of AIChE 2002 Annual Meeting, November 3–8, Indianapolis, IN; 2002:138e.
5. Wang Z, Kwauk M, Li H. Fluidization of fine particles. *Chem. Eng. Sci*. 1998;55:377-395.
6. Pacek AW, Nienow AW. Fluidisation of fine and very dense hard metal powders. *Powder Technol*. 1990;60:145-158.
7. Wang Y, Wei F, Jin Y, Luo T. Agglomerate particulate fluidization and E-particles. Proc. of the Third Joint China/USA Chem. Eng. Conf. (CUChE-3), 12-006, Beijing, China; 2000.
8. Wang Y, Gu G, Wei F, Wu J. Fluidization and agglomerate structure of SiO_2 nanoparticles. *Powder Technol*. 2002;124:152-159.
9. Nam C, Pfeffer R, Dave RN, Sundaresan S. Aerated vibrofluidization of silica nanoparticles. *AIChE J*. 2004;50:1776-1785.
10. Quevedo JA, Fluidization of Agglomerates of Nanoparticles Under Different Force Fields. Masters Thesis. NJIT, 2004.
11. Zhou T, Li H. Estimation of agglomerate size of cohesive particles during fluidization. *Powder Technol*. 1999;101:57-62.
12. Jung J, Gidaspow D. Fluidization of nano-size particles. *J. Nanoparticle Res*. 2002;4:483-497.
13. Li H, Hong R, Wang Z. Fluidizing ultrafine powders with circulating fluidized bed. *Chem. Eng. Sci*. 1999;54:5609-5615.
14. Wang Y, Wei F, Yu H, Gu G. The large-scale production of carbon nanotubes in a nano-agglomerate fluidized-bed reactor. *Chem. Phys. Lett*. 2002;364:568-572.
15. Matsuda S, Hatano H, Tsutusmi A. Ultrafine particle fluidization and its application to photocatalytic NO_x treatment. *Chem. Eng. J*. 2001;82: 183-188.
16. Zhou T, Li H. Force balance modeling for agglomerating fluidization of cohesive particles. *Powder Technol*. 2000;111:60-65.
17. Wang Y, Wei F, Jin Y, Luo T. Bed collapse behavior of primary nanoparticles. In: Kwauk M, Li J, Yang W-C, eds. *Fluidization X*, Proc. 10th Eng. Found. Conf. Fluidization, Beijing, RN, China; 2001:477-484.
18. Zhu C, Liu G, Yu Q, Pfeffer R, Dave RN, Nam C. Sound assisted fluidization of nanoparticle agglomerates. *Powder Technol*. 2004;141: 119-123.
19. Yu Q, Quevedo JA, Pfeffer R, Dave RN, Zhu C. Enhanced fluidization of nanoparticles in an oscillating magnetic field. *Journal*. 2005: In press.
20. Petrovic D, Posarac D, Skala D. Hysteresis effects of minimum fluidization velocity in a draft tube airlift reactor. *Chem. Eng. Sci*. 1989; 44:996-998.
21. Heck J, Onken U. Hysteresis effects in suspended solid particles in bubble columns with and without a draft tube. *Chem. Eng. Sci*. 1987; 42:1211-1212.
22. Peng Y, Fan LT. Hysteresis in liquid–solid tapered fluidized beds. *Chem. Eng. Sci*. 1995;50:2669-2671.
23. Loezos PN, Costamgna P, Sundaresan S. The role of contact stresses and wall friction on fluidization. *Chem. Eng. Sci*. 2002;57:5123-5141.
24. Tsinontides SC, Jackson R. The mechanics of gas fluidized beds with an interval of stable fluidization. *J. Fluid Mech*. 1993;225:237-274.
25. Iwadate Y, Horio M. Prediction of agglomerate sizes in bubbling fluidized beds of group C powders. *Powder Technol*. 1998;100:223.
26. Fayed ME, Otten L. *Handbook of Powder Science and Technology.* New York, NY: Van Nostrand Reinhold; 1984.
27. Davis RH, Birdsell KH. Hindered settling of semidilute monodisperse and polydisperserse suspensions. *AIChE J*. 1988;34:123-129.
28. Romero JB, Johanson LN. Factors affecting fluidized bed quality. *Chem. Eng. Prog. Symp. Ser*. 1958;58:28-37.
29. Happel J. Viscous flow in multiparticle systems: Slow motion of fluids relative to beds of spherical particles. *AIChE J*. 1958;4:197-201.
30. Neale G, Epstein N, Nader W. Creeping flow relative to permeable spheres. *Chem. Eng. Sci*. 1973;28:1865-1874.
31. Fan LS, Zhu C. *Principles of Gas–Solid Flows* (Cambridge Series in Chemical Engineering). Cambridge, UK: Cambridge University Press; 1998.

Appendix

Drag force correction on a porous agglomerate in a swarm in creeping flow

From SEM analysis, it appears that most nanoparticle agglomerates have highly porous chainlike structures, and exist in the form of multistage subagglomerates. The primary (normally, <20 nm) nanoparticles form chainlike clusters, and these three-dimensional netlike structures agglomerate into simple subagglomerates of a size range between 1 and 100 μm, but typically around 20 to 40 μm, and then these subagglomerates group together to generate large, 100 to 400 μm, porous floclike agglomerates.[8,9] Even though it is well known that these large agglomerates are highly porous structures, with a typical porosity about 99% or higher, previous studies of nanoagglomerate fluidization have always assumed that the agglomerates are solid particles for the purposes of hydrodynamic analysis. Although some researchers point out that treating porous floclike nanoparticle agglomerates as solid particles may lead to oversimplification, no one has actually calculated the effect of the flow through the porous agglomerates of nanoparticles. Using a simple model, we estimate the drag force correction factor for the hydrodynamic force on a highly porous floclike agglomerate in a swarm of other similar agglomerates.

Based on the free surface cell model of Happel,[29] Neale et al.[30] proposed a model to evaluate the drag force F_{Dp} exerted on a permeable sphere in a swarm of permeable spheres in creeping flow (low Reynolds number)

$$F_{Dp} = 3\pi\mu d_a V\Omega_p \tag{A1}$$

where V is the superficial fluid velocity flowing through the swarm, and Ω is the drag force correction factor attributed to the permeability of the sphere and the effect of neighboring spheres, and is given by

$$\Omega_p = \frac{2\beta^2 + \frac{4}{3}\beta^2\eta^5 + 20\eta^5 - \frac{\tanh\beta}{\beta}(2\beta^2 + 8\beta^2\eta^5 + 20\eta^5)}{\left(2\beta^2 - 3\beta^2\eta + 3\beta^2\eta^5 - 2\beta^2\eta^6 + 90\beta^{-2}\eta^5 + 42\eta^5 - 30\eta^6 + 3 - \frac{\tanh\beta}{\beta}\left(-3\beta^2\eta + 15\beta^2\eta^5 - 12\beta^2\eta^6 + 90\beta^{-2}\eta^5 + 72\eta^5 - 30\eta^6 + 3\right)\right.} \tag{A2}$$

Here, β is a permeability-dependent dimensionless sphere radius

$$\beta = \frac{d_a}{2\sqrt{k}} \tag{A3}$$

where d_a is the sphere diameter, k is the permeability of single permeable sphere, and η is a bed voidage–dependent dimensionless parameter, defined as

$$\eta = (1 - \varepsilon_g)^{1/3} \tag{A4}$$

where ε_g is the bed voidage around the whole swarm.

For very large β (very low k) the hydrodynamic behavior of a permeable sphere in a swarm of permeable spheres is similar to that of a solid sphere in a swarm of solid spheres; therefore, as $\beta \to \infty$, Eq. A2 will reduce to Happel's formula for a solid sphere in a swarm of solid spheres

$$\Omega_s = \frac{2 + \frac{4}{3}\eta^5}{2 - 3\eta + 3\eta^5 - 2\eta^6} \tag{A5}$$

where Ω_s is the drag force correction factor for a solid sphere in a swarm of solid spheres arising from the effect of neighboring spheres. Thus, the drag force F_{Ds} can be expressed as

$$F_{Ds} = 3\pi\mu d_a V \Omega_s \tag{A6}$$

If we define Ω as the ratio of the drag force for a permeable sphere in a swarm of permeable spheres (F_{Dp}) to the drag force for a solid sphere in a swarm of solid spheres (F_{Ds}), we can obtain Ω by combining Eqs. A1 and A6

$$\Omega \equiv \frac{F_{Dp}}{F_{Ds}} = \frac{\Omega_p}{\Omega_s} \tag{A7}$$

Estimation of k and β for nanoparticle agglomerates

From Darcy's law, the pressure drop per unit length over a porous agglomerate is related to the superficial fluid velocity as

$$V = -\frac{k}{\mu}\frac{dP}{dz} \tag{A8}$$

If we assume that the single agglomerate represents a packed bed, and treat the subagglomerates as individual solid (impermeable to the gas) particles in this packed bed, we can apply the Ergun equation (for low Reynolds number) to obtain a relation between the pressure drop per unit length, the voidage, and the subagglomerate size as

$$\frac{dP}{dz} = 150\frac{(1 - \varepsilon_{g,sub})^2}{\varepsilon_{g,sub}^3}\frac{\mu V}{d_{sub}^2} \tag{A9}$$

Here, we define the volume fraction of gas (voidage) within the single large agglomerate but surrounding the subagglomerates (which are assumed to be solid) as $\varepsilon_{g,sub}$, and the size of the subagglomerate as d_{sub}. It should be noted that $\varepsilon_{g,sub}$ is the gas-phase volume fraction around the subagglomerates in a single porous nanoparticle agglomerate and is neither the gas-phase volume fraction for the entire fluidized bed, which is expressed as ε_g, nor the gas-phase volume fraction surrounding primary nanoparticles.

By combining Eqs. A8 and A9, we obtain a relation between the permeability k of a single porous agglomerate, the subagglomerate porosity $\varepsilon_{g,sub}$, and the subagglomerate size d_{sub}

$$k = \frac{\varepsilon_{g,sub}^3}{(1 - \varepsilon_{g,sub})^2}\frac{d_{sub}^2}{150} \tag{A10}$$

We can now calculate the permeability-related dimensionless agglomerate radius β from Eq. A3, as

$$\beta = \frac{1}{2\sqrt{\frac{\varepsilon_{g,sub}^3}{150(1 - \varepsilon_{g,sub})^2}}}\frac{d_a}{d_{sub}} \tag{A11}$$

Calculation results

The voidage $\varepsilon_{g,sub}$ is very difficult to determine, so we simply estimate it to be 0.5, which is typical for a loosely packed bed of solid particles.[26,31] We also choose d_{sub} to be 30 μm (the average subagglomerate size), which is also in good agreement with SEM measurements by Nam et al.[9] The size of the large agglomerates d_a is obtained from the calculated results of Table 3 and β is calculated using Eq. A11; once we obtain β, we can calculate the drag force correction factor from Eq. A7.

Table A1 presents the calculated results of the permeability-related dimensionless radius β for all of the 11 nanoparticles studied; all of the values of β are in the range of 50 to 260. Table A2 presents the calculated results of the drag force correction factor Ω for permeable agglomerates in a swarm. We select β as 58.8 and 258 (the lower and upper limit for the

Table A1. Permeability-Related Dimensionless Radius β for Nanoparticle Agglomerates

Powder	Primary Size (nm)	Agglomerate Size (μm)	Permeability Related Dimensionless Radius β
R974	12	211	60.9
R805	12	279	79.9
R104	12	245	67.9
R711	12	207	60.4
COK84	12	316	92.1
R106	7	201	58.8
A 300	7	296	86.5
R972	16	195	67.0
OX50	40	300 (estimated)	86.6
A 90	20	896 (measured)	258
TiO_2	21	195 (measured)	56.2

Table A2. Drag Force Correction Factors for Nanoparticle Agglomerates

	β = 58.8 (R106, APF)			β = 258 (A90, ABF)		
ε_g	Ω_p (Eq. A2)	Ω_s (Eq. A5)	$\Omega = \Omega_p/\Omega_s$ (Eq. A7)	Ω_p (Eq. A2)	Ω_s (Eq. A5)	$\Omega = \Omega_p/\Omega_s$ (Eq. A7)
0.5	30.3	37.9	0.79	36.1	37.9	0.95
0.6	16.1	18.9	0.85	18.3	18.9	0.97
0.7	9.06	10.1	0.89	9.89	10.1	0.98
0.8	5.22	5.60	0.92	5.54	5.60	0.98
0.9	2.96	3.11	0.97	3.08	3.11	0.99
1.0	0.98	1.00	0.98	1.00	1.00	1.00

11 nanoparticles), and vary ε_g between 0.5 and 1.0. The results show that for the lower limit of $\beta = 58.8$ (R106, APF nanoparticles), the correction factors Ω for the drag force vary between 0.79 and 0.98 and increase with increasing bed voidage ε_g; for the upper limit of $\beta = 258$ (A90, ABF nanoparticles), the correction factors Ω are all >0.95.

Thus, for ABF nanoparticles, and also for APF nanoparticles, which fluidize at very high bed expansions (high ε_g), it appears that the error in assuming that highly porous nanoparticle agglomerates behave as solid particles for the purposes of hydrodynamic analysis is small. This implies that the Richardson–Zaki and Ergun equations derived for solid particles should be applicable to these porous nanoparticle agglomerates.

Manuscript received Feb. 23, 2004, and revision received Jun. 3, 2004.